Rheology of magmas with bimodal crystal size and shape distributions: insights from analog experiments

Geochemistry Geophysics Geosystems G3

Article
Volume 12, Number 7
28 July 2011
Q07024, doi:10.1029/2011GC003606
ISSN: 1525-2027

Published by AGU and the Geochemical Society

Rheology of magmas with bimodal crystal size and shape distributions: Insights from analog experiments

C. Cimarelli
Department für Geo- und Umweltwissenschaften, Ludwig-Maximilians-Universität München, Theresienstrasse 41, D-80333 Munich, Germany (cimarelli@min.uni-muenchen.de)

A. Costa
Environmental Systems Science Centre, University of Reading, Reading RG6 6AL, UK

Also at Istituto Nazionale di Geofisica e Vulcanologia, Via Diocleziano 328, I-56126 Naples, Italy

S. Mueller and H. M. Mader
School of Earth Sciences, University of Bristol, Wills Memorial Building, Queens Road, Bristol BS8 1RJ, UK

[1] Magmas in volcanic conduits commonly contain microlites in association with preexisting phenocrysts, as often indicated by volcanic rock textures. In this study, we present two different experiments that investigate the flow behavior of these bidisperse systems. In the first experiments, rotational rheometric methods are used to determine the rheology of monodisperse and polydisperse suspensions consisting of smaller, prolate particles (microlites) and larger, equant particles (phenocrysts) in a bubble-free Newtonian liquid (silicate melt). Our data show that increasing the relative proportion of prolate microlites to equant phenocrysts in a magma at constant total particle content can increase the relative viscosity by up to three orders of magnitude. Consequently, the rheological effect of particles in magmas cannot be modeled by assuming a monodisperse population of particles. We propose a new model that uses interpolated parameters based on the relative proportions of small and large particles and produces a considerably improved fit to the data than earlier models. In a second series of experiments we investigate the textures produced by shearing bimodal suspensions in gradually solidifying epoxy resin in a concentric cylinder setup. The resulting textures show the prolate particles are aligned with the flow lines and spherical particles are found in well-organized strings, with sphere-depleted shear bands in high-shear regions. These observations may explain the measured variation in the shear thinning and yield stress behavior with increasing solid fraction and particle aspect ratio. The implications for magma flow are discussed, and rheological results and textural observations are compared with observations on natural samples.

Components: 8400 words, 7 figures, 3 tables.

Keywords: analog experiments; crystal bearing; magma; polydisperse suspensions; rheology.

Index Terms: 8429 Volcanology: Lava rheology and morphology; 8434 Volcanology: Magma migration and fragmentation; 8445 Volcanology: Experimental volcanism.

Received 4 March 2011; **Revised** 21 April 2011; **Accepted** 27 April 2011; **Published** 28 July 2011.

Cimarelli, C., A. Costa, S. Mueller, and H. M. Mader (2011), Rheology of magmas with bimodal crystal size and shape distributions: Insights from analog experiments, *Geochem. Geophys. Geosyst.*, *12*, Q07024, doi:10.1029/2011GC003606.

1. Introduction

[2] Magma generally consists of a polyphase suspension of crystals and gaseous bubbles in a liquid phase: the silicate melt. The fluid mechanics of magma in a volcanic conduit are therefore strongly influenced by the rheological changes that arise from microphysical processes such as vesiculation, degassing, and crystallization. Increases in crystal content can lead to a dramatic increase in the viscosity of the magmatic suspension (melt + bubbles + crystals).

[3] During ascent, magma can undergo a complex history of crystallization. Crystals can originate from supercooling, increase in the liquidus temperature due to water exsolution, or from vesiculation induced by pressure changes [*Szramek et al.*, 2006; *Toramaru et al.*, 2008; *Suzuki and Fujii*, 2010]. Hence, it is not uncommon in volcanic rocks to find microlites in association with preexisting phenocrysts which nucleated in the magma chamber or in deeper portions of the volcano plumbing system. Such bimodal crystal size distributions suggest that microlite formation is a shallow process typical of the last stages of magma evolution prior to eruption [*Hammer et al.*, 1999; *Noguchi et al.*, 2006]. Progressive increase of microlite volume percentage can dramatically affect the rheology of rising magma within the conduit consequently affecting eruptive style. This process is relevant over a broad spectrum of magma compositions [*Sparks*, 1997; *Houghton and Gonnermann*, 2008]. In particular the low viscosity of high temperature basaltic melts can be subject to notable rheological changes (more than an order of magnitude) when crystallization of microlites takes place [*Ishibashi and Sato*, 2007; *Vona et al.*, 2011]. Moreover, textural observations of tephra from recent basaltic explosive eruptions suggest that the increased viscosity and propensity for brittle fragmentation of microlite-rich magmas may control the transition from mild to violent basaltic eruptions [*Sable et al.*, 2006; *Andronico et al.*, 2009; *Cimarelli et al.*, 2010].

[4] The rheology of very concentrated suspensions (i.e., suspensions with particle concentrations above the critical solid volume fraction) and crystal-bearing magmas has been investigated both experimentally [e.g., *Pinkerton and Stevenson*, 1992; *Lejeune and Richet*, 1995; *Petford*, 2003] and theoretically [see, e.g., *Costa*, 2005; *Costa et al.*, 2009]. The rheology of crystal bearing magmas, like that of very concentrated suspensions is mainly controlled by the solid fraction [e.g., *Lejeune and Richet*, 1995; *Costa et al.*, 2009], applied strain rate [e.g., *Caricchi et al.*, 2007; *Costa et al.*, 2009], particle aspect ratio [*Mueller et al.*, 2010] and particle size distribution [*Farris*, 1968; *Chong et al.*, 1971]. Theoretical and experimental studies of polymodal particle distributions have so far mainly been restricted to the description of ideal cases of suspensions of spherical particles with different diameters [*Farris*, 1968; *Chong et al.*, 1971]. Although shape polymodality is a common feature of geophysical fluids such as magma and debris flows, and also of suspensions of industrial interest (food industry, mold industry, etc.), this feature has been even less investigated. *Marti et al.* [2005] focused on the rheology of concentrated suspensions of spheres and fibers, where the fiber diameter was chosen to correspond to the diameter of the spheres and their length to be one order of magnitude larger. Their experimental results are satisfactorily described using an approach similar to the one used by *Farris* [1968], in which the system is treated as a suspension of coarser particles in a viscous medium made of a liquid containing finer particles.

[5] The experiments presented here are designed as analog for studying the role of increasing microlite content on the rheology of a magma with different starting amounts of phenocrysts. The suspensions were generated by adding different proportions of smaller prolate particles to a fixed amount of larger isometric ones in a bubble-free Newtonian liquid. In this way the increasing total solid volume fraction is dependent on the progressive relative abundance of fines with respect to the fixed percentage of coarse particles. Here, we aim to describe the flow behavior of suspensions composed of particles having different size and shape as a function of their solid fractions. We do this by modeling experimental data using semi empirical parameterizations, such as *Krieger and Dougherty* [1959] and *Costa et al.* [2009], thus testing the applicability of *Farris*'s [1968] approach for more general particle aspect ratios and strain rate conditions than those investigated by *Marti et al.* [2005]. We also use textural observations to understand the influence of the interaction between particle populations and their spatial rearrangement on the rheology of the suspensions under shear flow conditions.

2. Analog Materials and Experimental Apparatus

[6] Following the experimental procedure of *Mueller et al.* [2010], rheology measurements were

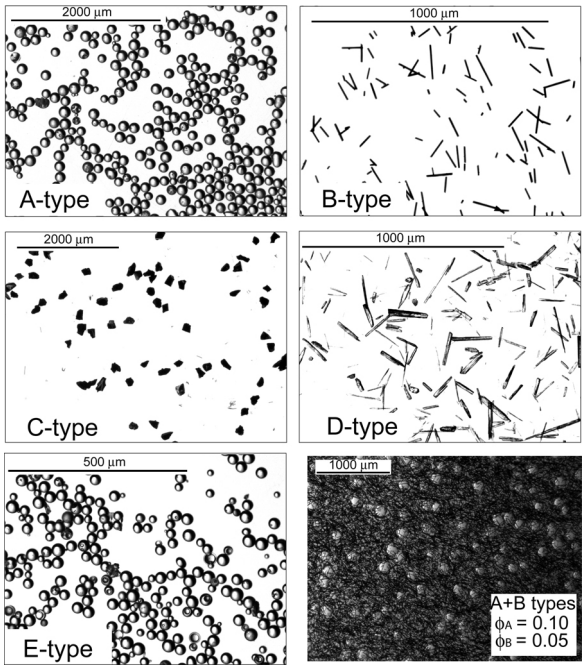

Figure 1. Stereomicroscope photographs of the particles employed in the experiments: A type (coarse-grained glass beads), B type (carbon fibers), C type (silicon carbide grit), D type (wollastonite crystals), E type (fine-grained glass beads), and A+B particles blend with ϕ = 0.1 A-type particles and ϕ = 0.05 B-type particles. Note that the thickness of the volume of the A+B bimodal suspension portrayed is about 250 μm.

performed on suspensions of particles with different geometries immersed in a Newtonian silicone oil. The silicone oil employed in the experiments is a calibration oil with viscosity of 41.32 Pa s and density of 894 kg/m^3 at 25°C. The silicone oil used shows a Newtonian behavior over the range of stress (0–500 Pa) and strain rates (10^{-4} − 1 s^{-1}) investigated in this work. Although the viscosity of a given melt can span several orders of magnitude according to its temperature, the viscosity of the silicone oil is within the range expected for low viscosity magmas at subliquidus temperature [*McBirney and Murase*, 1984; *Spera*, 2000; *Giordano et al.*, 2008].

[7] The solid particles used were glass beads (isometric; Figure 1 (type A and E) and Table 1), carbon fibers (prolate; Figure 1 (type B) and Table 1), SiC grit (equant; Figure 1 (type C) and Table 1) and wollastonite crystals (prolate; Figure 1 (type D) and Table 1). The particles were chosen in order (1) to resemble the shapes and the dimensions of natural equant phenocrysts and prolate microlites, (2) to display uniform particle size distributions among the respective type of particles, and (3) to have a similar density to the silicone oil in order to avoid settling during the experiments. Moreover, SiC and wollastonite particles, which display roughly the same aspect ratios of glass beads and carbon fibers, respectively, have been chosen in order to investigate the effect of angular surfaces resembling that of natural crystals on the flow properties of the suspended solid fraction. All the particles have been optically characterized by measuring their long and short axes or diameter. Images were taken under a stereomicroscope and particles were measured via image analysis.

[8] In order to produce suspensions with a well-defined particle concentration, the silicone oil and particles were mixed according to their weight; the corresponding volume fractions were then calculated using the respective particles and oil densities. In order to remove bubbles entrained in the mixture, the samples were centrifuged for at least 1 h at 4000 rpm at room temperature. Subsequently the samples were carefully stirred until the two phases were homogeneously distributed. The fact that the two types of particles displayed contrasting colors with respect to the transparent silicone oil helped to

Table 1. Particle Types and Their Properties[a]

	A	B	C	D	E
Geometry	spherical	prolate	angular equant	angular prolate	spherical
Material	glass beads	carbon fibers	SiC grit	wollastonite	glass beads
Density	2448 kg/m^3	1740 kg/m^3	3166 kg/m^3	2750 kg/m^3	2448 kg/m^3
Min–max l	32–159 μm	5–695 μm	4–922 μm	22–292 μm	19–66 μm
Mean l	125.73 μm	72.38 μm	251.32 μm	72.26 μm	47.64 μm
σ_l	17.58	52.22	110.16	38.69 μm	8.79 μm
Min–max w	30–157 μm	8.00 μm	4–647 μm	3–35 μm	18–66 μm
Mean w	122.27	8.00 μm	156.22 μm	9.81 μm	46.25 μm
σ_w	17.43	-	66.25	5.04 μm	8.73 μm
Min–max r	1–1.32	0.11–86.92	1.82–15.51	0.98–32.96	1–1.68 μm
Mean r	1.03	9.05	1.82	8.50	1.06 μm
σ_r	0.03	6.53	1.08	4.76	0.06 μm

[a]The l is the particle length, w is the width, r is the aspect ratio l/w, and σ denotes the standard deviation of the different parameters.

understand when the solid phase was homogenously distributed. In order to obtain the maximum particles fraction packing, excess volume of particles was added to the liquid and, after having centrifuged the sample, nonwet particles in excess were removed. In centrifuged samples reaching the maximum packing, bidisperse particles appeared layered according to their density (i.e., beads at the bottom and fibers at the top). In order to be homogenized, the samples were carefully wrapped in a plastic film and squeezed and folded until a homogeneous paste was obtained.

[9] Rheological measurements were performed by running controlled shear stress tests on a Thermo-Haake MARS II rotational rheometer fitted with a parallel plate sensor system with a plate diameter of 35 mm and a gap between the plates of 1.5 mm to allow for the size of coarser particles. The rheological measurements involved two stages: (1) preshear treatment of the sample and (2) the rheometric determination. The preshear treatment involves shearing the sample from 0 to 150 Pa then back again. This has the purpose of eliminating transient rheological effects due to partial settling, reorientation and organization of the particles within the liquid, thereby ensuring repeatable measurements thereafter. The rheometric determination is the main measurement and consists of increasing (up ramp) and decreasing (down ramp) the stress value through steps of 25 Pa. During each step, a constant stress is applied and the corresponding strain rate is recorded until it reaches a constant value. The maximum applied stress has been set to 500 Pa. The stress increment is 25 Pa for all measurements, so that the number of steps is proportional to the maximum stress and total strain reached in each experiment.

[10] We characterize the suspensions in terms of the volume solid fraction ϕ, which represents the ratio of the volume of solids (V_s) versus the volume of solids plus liquid ($V_s + V_l$): $\phi = V_s/(V_s + V_l)$. When dealing with bimodal suspensions, where the volume solid fraction consists of both coarser (V_c) and finer (V_f) particles, as by *Farris* [1968], we define ϕ_c as the ratio of the volume of coarse particles versus the total volume of the suspension: $\phi_c = V_c/(V_c + V_f + V_l)$, and $\phi_f = V_f/(V_f + V_l)$, i.e., the volume of fine particles on the volume of small particles plus liquid.

[11] We considered the following polymodal blends:

[12] 1. A+B blend, i.e., spherical beads + carbon fibers. For this case, three different sets of experiments were performed in which a progressively increasing percentage of fibers were added, maintaining a fixed amount of coarser spherical particles (ϕ_c = 0.1, 0.2, and 0.3, respectively).

[13] 2. C+D blend, i.e., SiC grit (angular, quasi-isometric) + wollastonite (angular, prolate). Being natural crystals characterized by angular surfaces, this case investigates the effect of particle roughness on flow properties. Rough particles were chosen with the same average physical dimension as the smooth ones used in the A+B blends.

[14] 3. A+E blend, i.e., bimodal suspension of coarse and fine spherical beads. This case was investigated also for a comparison with previous theoretical and experimental studies. The experiments performed on polymodal blends of spheres and fibers were compared to their monodisperse counterparts.

[15] Finally, we used epoxy resin as a liquid phase in an A+B blend in order to be able to freeze the suspension after deformation in a concentric cylinder setup. This allowed us qualitatively to investigate the microstructures generated by the rearrangement of the solid phase during the deformation of the suspensions and to help interpret the results obtained by the rheological measurements.

3. Rheological Measurements and Data Modeling

3.1. Used Parameterizations

[16] Data points derived from rheological measurements are commonly described by fitting the parameters of *Herschel and Bulkley*'s [1926] equation, for the stress (τ) − strain rate ($\dot{\gamma}$) relationship:

$$\tau = \tau_0 + K\dot{\gamma}^n \quad (1)$$

thus obtaining a value of consistency K, flow index n and yield stress τ_0 for each tested suspension. We estimate K, n and τ_0, from measurement data of stress versus strain rate for each sample characterized by a given particle volume fraction ϕ. The deviation from Newtonian behavior (i.e., from $\tau_0 = 0, n = 1$) increases as the particle shape deviates from spherical as described by *Mueller et al.* [2010].

[17] In order to account for the combined effect of solid fraction, strain rate and particle shape we use the concept of effective relative viscosity (ratio between the effective viscosity of the solid-liquid suspension and the viscosity of the liquid phase).

Following from equation (1), the effective relative viscosity is defined as

$$\eta_r \equiv \frac{1}{\mu_l}\left(\frac{\tau - \tau_0}{\dot{\gamma}}\right) = \frac{K\dot{\gamma}^{n-1}}{\mu_l} \quad (2)$$

where μ_l represents the viscosity of the liquid phase and η_r a dimensionless quantity which reduces to the classical relative viscosity as $n = 1$.

[18] Several parameterizations have been proposed in the geologic and engineering literature for describing the effective viscosity η as a function of the solid fraction ϕ, i.e., $\eta = \eta(\phi)$. Here, we restrict our analysis and discussion to two semiempirical parameterizations only: the parameterization by *Krieger and Dougherty* [1959] which contains only one adjustable parameter and *Costa et al.* [2009] parameterization which uses three fitting parameters. As we will show below, in the framework of semiempirical models, *Krieger and Dougherty*'s [1959] parameterization works well for diluted suspension even for nonequant particles, however the description of the rheology of concentrated suspensions need a larger number of adjustable parameters. For a broader discussion of rheological models and other approaches describing effective viscosity of concentrated particle suspensions of geological and industrial interest, we would like to refer to the recent reviews of *Petford* [2003, 2009] and *Stickel and Powell* [2005].

[19] For monodisperse suspensions, *Krieger and Dougherty* [1959] considered the contribution of successive parcels of the suspension to the total particle volume fraction and to the suspension viscosity obtaining the following relationship:

$$\eta_r(\phi) = \left(1 - \frac{\phi}{\phi_m}\right)^{-B\phi_m} \quad (3)$$

where B is the Einstein coefficient and ϕ_m represents the critical solid fraction at which the viscosity, mathematically, tends to infinity. Commonly B and ϕ_m are used as fitting parameters. The critical fraction ϕ_m strongly depends on the particle aspect ratio [*Mueller et al.*, 2010], strain rate [*Caricchi et al.*, 2007; *Costa et al.*, 2009] and particle dispersion [*Farris*, 1968; *Marti et al.*, 2005].

[20] A semiempirical parameterization of the relative viscosity, valid for concentrated suspensions was proposed by *Costa* [2005] and then modified by *Costa et al.* [2009]:

$$\eta_r(\phi) = \frac{1 + \left({}^{\phi}/_{\phi*}\right)^{\delta}}{\left[1 - F\left(\frac{\phi}{\phi*}, \xi, \gamma\right)\right]^{B\phi*}} \quad (4)$$

where $F = (1 - \xi)\ \mathrm{erf}\left[\frac{\sqrt{\pi}}{2(1-\xi)}\frac{\phi}{\phi*}\left(1 + \frac{\phi^{\gamma}}{\phi*^{\gamma}}\right)\right]$. The parameter $\phi*$ represents the critical solid fraction at which the rheological transition from a dominant liquid phase regime switches to a regime where the effect of crystals is predominant and the viscosity values are much higher [*Costa*, 2005; *Costa et al.*, 2009]. While the parameter γ is a measure of the rapidity of relative viscosity increase with crystal fraction as ϕ approaches $\phi*$, the parameter δ controls the increase of η_r at $\phi > \phi*$. As in the work by *Costa et al.* [2009] we set $\delta = 13 - \gamma$. The parameter ξ determines the values of η_r at $\phi = \phi*$: $\eta* = \eta_r(\phi*) = 2 \cdot [1 - (1 - \xi) \cdot \mathrm{erf}(\sqrt{\pi}/(1 - \xi))]^{-B\cdot\phi*}$. For a more detailed description of the model see *Costa et al.* [2009].

[21] For the case of bidisperse suspensions, *Farris* [1968] treated the system as a coarse solid fraction suspended in a fluid containing the finer particles. In the work by *Farris* [1968], coarser and finer fractions have the same shape and behave independently of each other: $\eta_r = \eta_r(\phi_c)\eta_r(\phi_f)$.

3.2. Modeling of Rheological Measurements

[22] Flow properties of bimodal suspensions depend on the contribution of the different populations of solid particles immersed in the liquid, therefore it is here useful to examine the behavior of monodisperse suspensions of the particles that were used to blend the bimodal suspensions. Hence, for sake of comparison, Figure 2 shows the effective relative viscosity, the flow index and the yield stress of suspensions made of A-, B-, C- and D-type particles.

[23] The values of effective relative viscosity for strain rates of 10^{-4} s^{-1} and 1 s^{-1} (equation (1)) are fitted using equation (3) [*Krieger and Dougherty*, 1959] and equation (4) [*Costa et al.*, 2009]. Best fit parameters are reported in Table 2.

[24] The *Krieger and Dougherty* [1959] model is able to fit the data points appropriately only in the low concentration regions, especially in the case of prolate particles, whereas the *Costa et al.* [2009] model performs much better. It is worth mentioning that, as there are few measurements in the high concentration region ($\phi > \phi*$) the adjustable parameters γ and ξ, derived from the nonlinear fitting of equation (4), are not very well constrained. The global optimum can be not very well characterized, and the solution can get stuck at a local minimum. Curve values for solid fractions larger than the

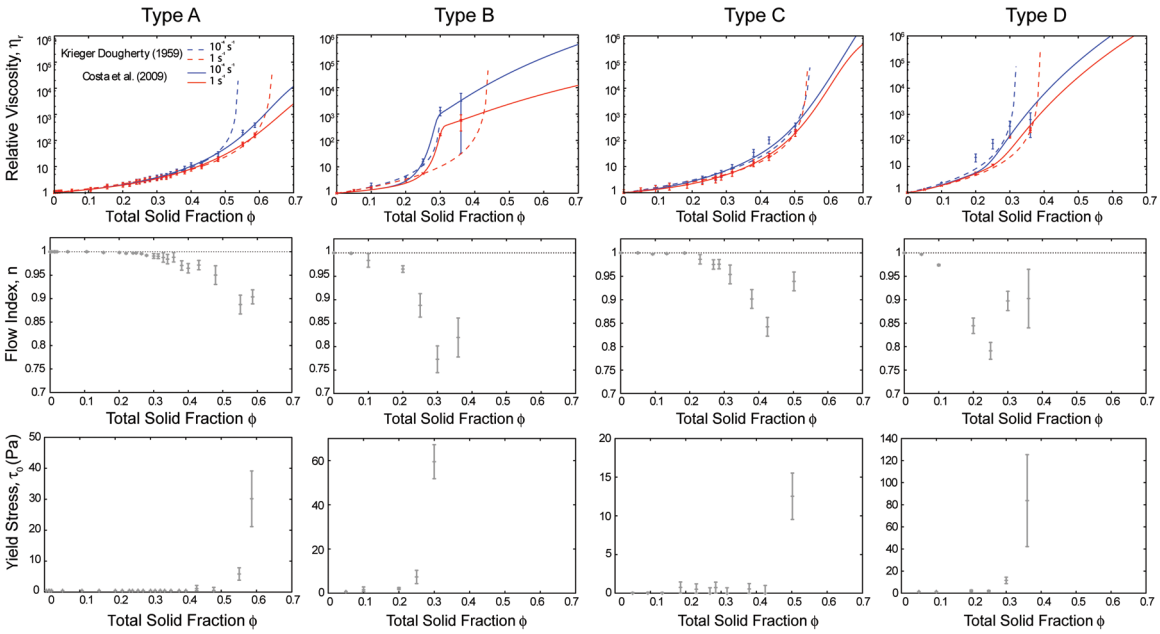

Figure 2. Effective relative viscosity (η_r), the flow index (n), and the yield stress (τ_0) of monodisperse suspensions made of A-type particles (spheres), B-type particles (fibers), C-type particles (grit), and D-type particles (wollastonite). Relative viscosity values and fitting curves were calculated using the model of *Costa et al.* [2009] for strain rates of 10^{-4} (solid blue lines) and 1 s^{-1} (solid red lines), respectively. For the same strain rate values the results deriving from *Krieger and Dougherty* [1959] model (blue and red dashed lines, respectively) are shown for comparison. Dotted line of flow index $n = 1$ is shown for reference.

measured ones, although consistent in terms of order of magnitude with previous studies [*Costa et al.*, 2009], should be considered as extrapolations.

[25] Figure 3 reports the results obtained for three kinds of bidisperse blends where the volume fraction of coarse particles was set to $\phi_c = 0.1$. Figure 4 the behavior of blend made of A+B particles is shown for different constant coarse particle fractions set to $\phi_c = 0.1$ (as in Figure 3), $\phi_c = 0.2$ and $\phi_c = 0.3$, respectively.

[26] As well as in the case of monodisperse blends, the values of effective relative viscosity for strain rates of 10^{-4} s^{-1} and 1 s^{-1} fitted using equation (3) and equation (4) are also reported (for the best fit parameters see Table 3). Also in the bidisperse cases, due to the few data points in the region of high particle concentration ($\phi > \phi_*$), the adjustable parameters γ and ξ are not very well constrained, but in general the *Costa et al.* [2009] parameterization shows a good performance. Differently from results by *Marti et al.* [2005], parameterization by *Krieger and Dougherty* [1959] is able to reproduce data points in the low particle concentration regions only, and it is clear that best fit values of ϕ_m do not represent a real critical solid fraction (Figures 3 and 4).

[27] Examining Figure 2 and Figure 3, it is possible to note that the extent of the deviation from Newtonian behavior varies depending on the fraction of finer elongated particles and on the aspect ratio of the particle type. Notably, for suspensions containing high aspect ratio particles, a substantial discrepancy of values of the flow parameters τ_0 and

Table 2. Best Fit Parameters of Equation (3) and Equation (4) for Monodisperse Suspensions

	A		B		C		D	
Strain rate (s^{-1})	10^{-4}	1	10^{-4}	1	10^{-4}	1	10^{-4}	1
ϕ_m	0.54	0.61	0.36	0.44	0.47	0.54	0.32	0.39
$B\phi_m$	1.64	2.00	1.75	2.03	2.05	2.01	2.15	2.13
ϕ_*	0.62	0.67	0.26	0.28	0.51	0.54	0.24	0.28
γ	1.52	1.60	5.50	8.55	0.69	1.32	0.10	0.11
$\xi \times 10^{-3}$	5	10	0.2	1	0.05	0.5	30	21

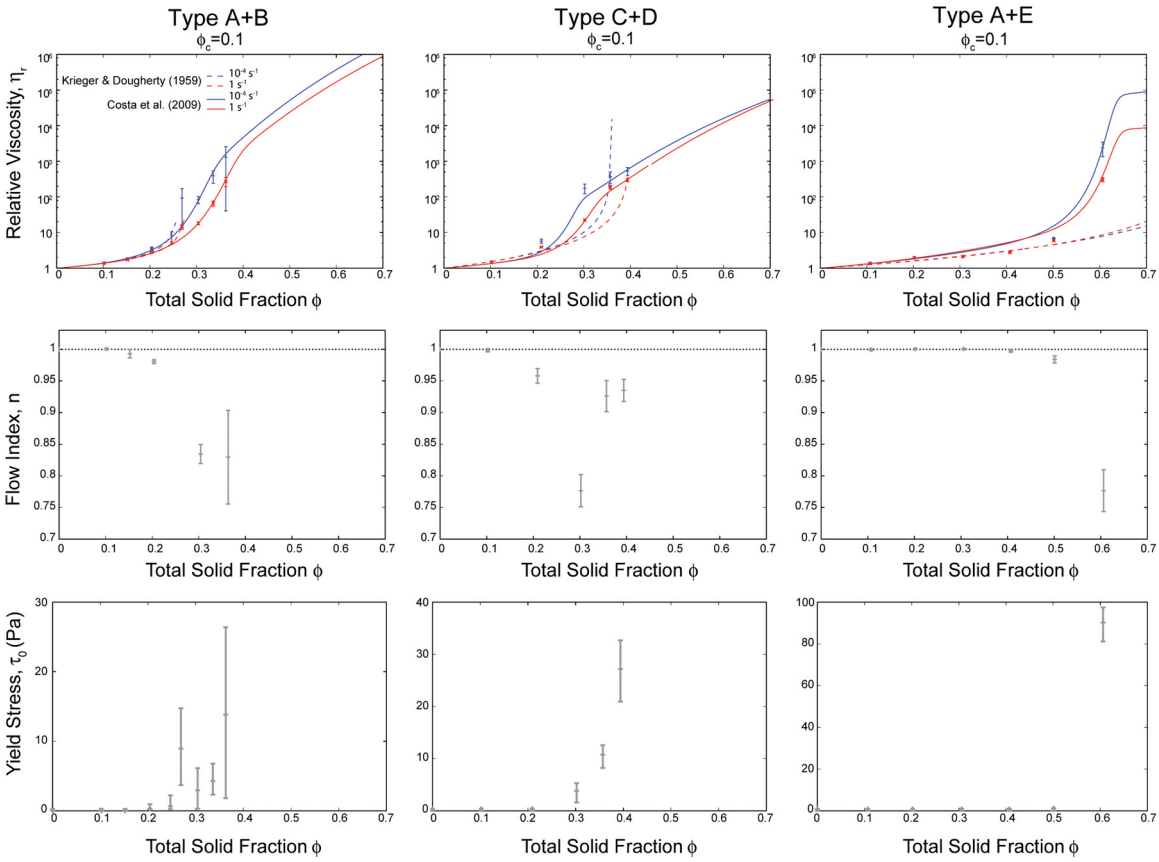

Figure 3. Effective relative viscosity (η_r), the flow index (n), and the yield stress (τ_0) of suspensions made of A+B type particles (spheres and fibers), C+D type particles (SiC and wollastonite), and A+E type particles (large and small spheres). Fraction relative to the coarser particles was maintained constant to ϕ_c = 0.1 for all three cases. Relative viscosity values and fitting curves were calculated using the model of *Costa et al.* [2009] for strain rates of 10^{-4} s^{-1} and 1 s^{-1} (blue and red solid lines, respectively). For the same values of strain rate the results deriving from *Krieger and Dougherty*'s [1959] model (blue and red dashed lines, respectively) are shown for comparison. Dotted line of flow index n = 1 is shown for reference.

n is registered during the up- and down-ramp measurements, as testified by the wider error bars of data points at high solid concentration. For the concentrated mixtures, the shear stress–shear rate relation is not identical when measured with increasing or decreasing stress. Hysteresis of the flow curve [*Balmforth and Craster*, 2001] is such that, for a given shear stress, values of shear rate are systematically lower on the down ramp than on the up ramp. In this work we do not account for such hysteresis effect as we use the averaged up-down values as the basis for fitting the curves. It is, however, important to bear in mind this effect in considering the representativeness of relative viscosity averaged value as hysteresis effects become more relevant at concentrations close to the maximum packing. Nonetheless, the difference between values obtained for the up- and down-ramp at maximum packing concentrations ranges between 20 and 30% (the biggest discrepancy of 30% is obtained for A+B blends at ϕ = 0.36).

[28] For the case of A+B blends we plotted the effective relative viscosities as a function of fiber fraction (Figure 5). In Figure 5 dotted and dashed lines represent values calculated using *Farris*'s [1968] approach, and points represent experimental data corresponding to a shear rate of 1 s^{-1}. Both *Krieger and Dougherty* [1959] parameterization (dotted lines) and *Costa et al.* [2009] parameterization (dashed lines) were used for best fitting the experimental data using values of the maximum packing previously found for the spheres and the fibers. It is clear from Figure 5 that the performance of *Farris*'s [1968] approach for this kind of systems is relatively poor. A better performance is given by the *Costa et al.* [2009] model with the

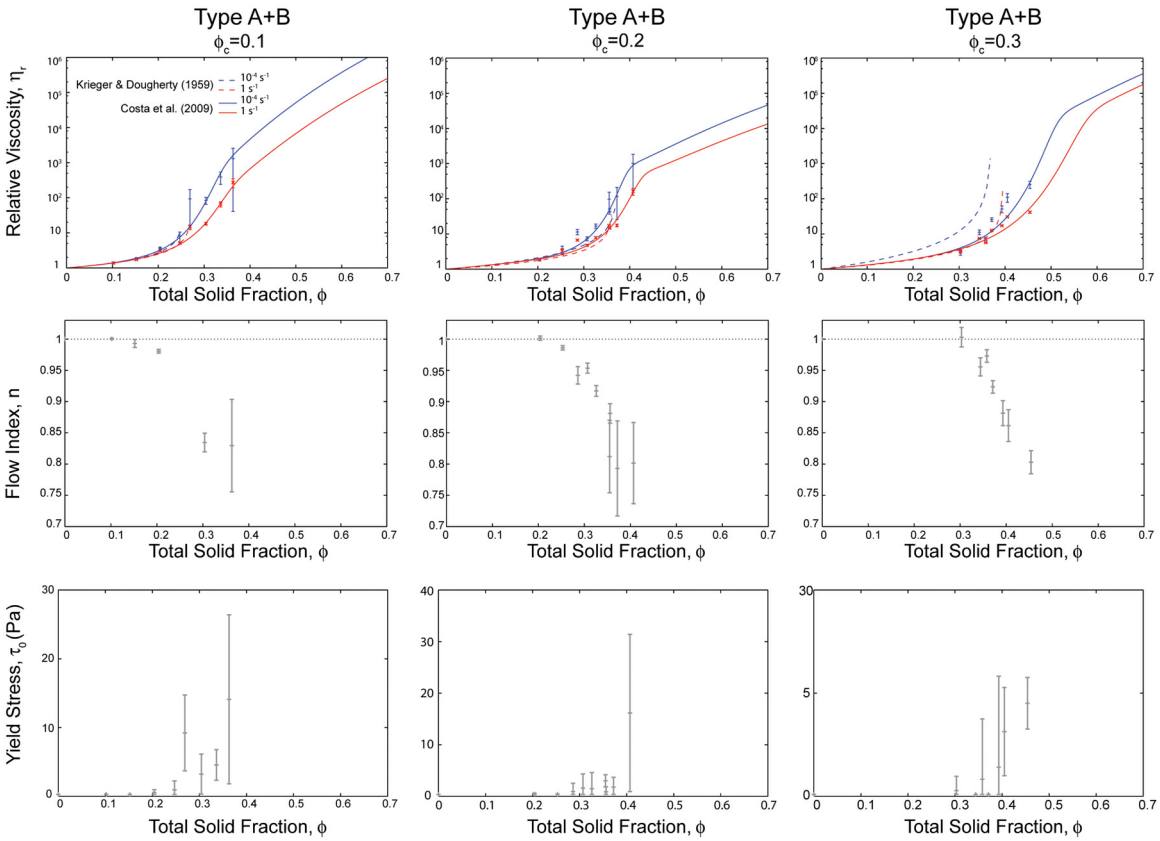

Figure 4. Effective relative viscosity (η_r), the flow index (n), and the yield stress (τ_0) of suspensions made of A+B type particles (spheres and fibers). Variable proportions of coarser spheres have been used ϕ_c = 0.1, 0.2, and 0.3, respectively. Relative viscosity values and fitting curves were calculated using the model of *Costa et al.* [2009] for strain rates of 10^{-4} s^{-1} and 1 s^{-1} (blue and red solid lines, respectively). For the same values of strain rate the results deriving from *Krieger and Dougherty* [1959] model (blue and red dashed lines, respectively) are shown for comparison. Dotted line of flow index n = 1 is shown for reference.

adjustable parameters of the A+B blend obtained interpolating the fitting parameters for the monodisperse cases A and B, according to the following relationships:

$$\begin{aligned}\phi_{*AB} &= \phi_{*B}x^{1.34} + \phi_{*A}(1-x)^{1.34}\\ \gamma_{AB} &= \gamma_B x + \gamma_A(1-x)\\ \xi_{AB} &= \xi_B x + \xi_A(1-x)\end{aligned} \tag{5}$$

where ϕ_{*A}, γ_A, ξ_A and ϕ_{*B}, γ_B, ξ_B are the adjustable parameters independently found for an A-type and a B-type suspension, respectively, and x is the fraction of finer to coarser particles ($x = \phi_f/(\phi_f + \phi_c)$).

[29] Increasing the solid fraction, the viscosity of elongated particles increases faster than that of spherical particles (see Figure 2). This trend is shown also in bidisperse blends. Figure 5 shows that for a constant value of solid fraction (e.g., ϕ = 0.3), the relative viscosity of the suspension increases as a function of the increasing proportion of finer elongated particles.

[30] For higher solid fractions, the transition in the behavior from sphere-like blend to fiber-like blend is more abrupt. To stress out the role of shape polymodality, it is convenient to compare Figure 5 of this work with Figure 12 of *Chong et al.* [1971]. In their work, *Chong et al.* [1971] report the relative viscosity (η_r) of blends of spherical particles having different diameters. They note that generally for 0.25 < ϕ_f < 0.35, η_r reaches its minimum value, while at ϕ_f = 0 and ϕ_f = 1, η_r reaches the

Table 3. Best Fit Parameters of Equation (3) and Equation (4) for Bidisperse Suspensions With Fixed Coarse Fraction at ϕ_c = 0.1

	A+B		C+D		A+E	
Strain rate (s^{-1})	10^{-4}	1	10^{-4}	1	10^{-4}	1
ϕ_m	0.25	0.27	0.36	0.40	0.94	0.84
$B\phi_m$	0.65	0.69	1.30	1.46	2.0	1.69
ϕ_*	0.30	0.33	0.28	0.25	0.60	0.62
γ	2.14	2.28	4.99	3.95	9.0	10.4
$\xi \times 10^{-3}$	1	5	6	10	1	5

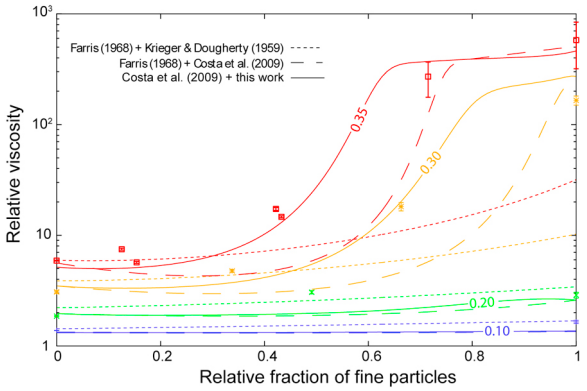

Figure 5. Relative effective viscosity as a function of fraction of fibers for A+B particle blends (spheres and fibers) for ϕ = 0.10 (blue), ϕ = 0.20 (green), ϕ = 0.30 (yellow), and ϕ = 0.35 (red). Points represent experimental data corresponding to a shear rate of 1 s^{-1}. Dashed lines represent calculated values using *Farris*'s [1968] approach with *Costa et al.*'s [2009] parameterization, dotted lines represent calculated values using *Farris*'s [1968] approach with *Krieger and Dougherty* [1959], and solid lines represent *Costa et al.*'s [2009] parameterization with interpolated parameters.

same maximum value (as they used only populations of spheres with different diameter). In this way the function $\eta_r(\phi_f)$ describes a quasi-symmetric curve concave upwards. We note that in our case there is no symmetric behavior and η_r reaches a minimum when $\phi_f = 0$ while it gets to maximum values for ϕ_f approaching 1 (i.e., when elongated particles prevail).

3.3. Textural Observations

[31] To help understand the rheological results we need to visualize the microstructure created by the interaction of the particle populations in the flow. In order to do so we reproduced the simple shear conditions of the A+B type suspension (with ϕ = 0.1 for the spheres and ϕ = 0.2 for the fibers) in a concentric cylinder geometry (Figure 6a). The particles were immersed in epoxy resin (viscosity of 200 mPa s and density of 1058 kg/m^3 at 25°C) and deformed at a very low shear rate (strain rate ~10^{-2} s^{-1}; total strain ~10^2) at room temperature for about one hour. After shearing, the whole mixture has been let solidify under the effect of the

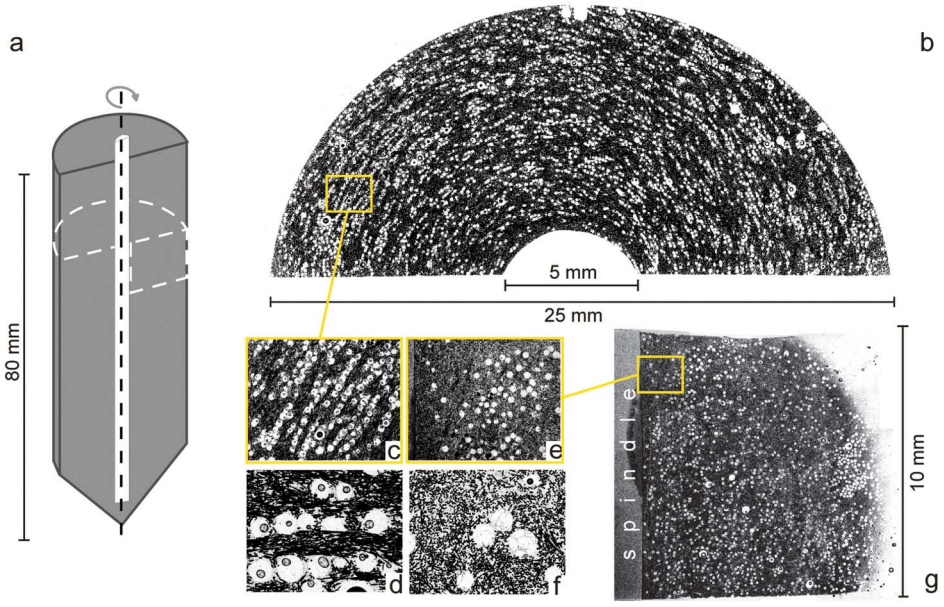

Figure 6. Here we show results of the experiments using A (ϕ = 0.1) plus B (ϕ = 0.2) blend and transparent epoxy resin as liquid phase. The suspension has been deformed in (a) a concentric cylinder setup, and once solidified, sectioned (b) perpendicular and (g) parallel to the spindle axis (black dotted line). White spots are the glass beads immersed in a matrix of black carbon fibers and transparent epoxy. On the plane perpendicular to the spindle axis the spheres are well organized in (c) "string of pearls" structures separated by spheres-depleted bends of fibers aligned according to (d) the flow field. (e) Along the plane containing the spindle axis and perpendicular to the shear direction the spheres do not show such organization, while (f) the fibers are aligned according to the flow field (perpendicular to image) and appear as small black dots. In Figures 6b and 6g the impoverishment of spheres closer to the spindle is evident, i.e., where the shear rate is higher.

curing agent of the resin (approximate time of curing after mixing 6–7 h). Once solidified, the mixture was removed from the container and sectioned perpendicular (Figure 6b) and parallel (Figure 6g) to the spindle axis thus enabling its textural analysis. It is worth remarking that, given the high concentration of suspended particles (very close to the maximum random packing) and their low density contrast respect to the epoxy, settling of particles during the curing time can be considered negligible, as also shown by Figure 6 that shows how the particles are uniformly distributed in the liquid. Moreover, in order not to induce disturbances in the particle arrangement, the spindle was not removed before the mixture had solidified, and was then sectioned together with the sample.

[32] The two sections show contrasting features. In the section parallel to the spindle axis and perpendicular to the shear direction (Figure 6g), the black carbon fibers show a preferential orientation perpendicular to the section plane and appear as small black dots as they are sectioned perpendicular to their long axis (Figure 6f). In the same plane, the larger glass spheres do not show any particular organization (Figure 6e). By contrast, in the section perpendicular to the spindle axis (Figure 6b), both fine and coarse particles are well aligned tangentially between the spindle and the outer cylinder. As expected, the fibers are aligned with their long axis parallel to the flow lines. It is remarkable how the glass beads, which, due to their spherical symmetry, always expose a minimum resistance profile in the flow, are well organized in "string of pearls" structures (Figure 6c). Such structures are formed by touching particles (longest structures include up to 11 particles in the same plane) aligned along the flow field, i.e., tangential to the spindle and the outer cylinder. Fibers are homogeneously distributed and fill the space between the spheres strings, forming sphere depleted bands of variable thickness (Figure 6d). Combining the two perpendicular sections it is also possible to note that the portion of suspension more proximal to the spindle, where the shear is maximum, is depleted of larger particles (Figures 6e and 6g).

4. Discussion of Experimental Results and Implications for Natural Magmas

[33] Our results are in qualitative agreement with previous theoretical and experimental studies on the rheology of analog suspensions and on natural magmas. In particular, they confirm the influence of particle concentration and shape on the deviation from Newtonian behavior [*Mueller et al.*, 2010]. Such effects are more evident for particles with higher aspect ratios, as in the case of elongated crystals in natural magmas [*Ishibashi*, 2009; *Vona et al.*, 2011].

[34] As shown by experiments on monodisperse suspensions (Figure 2), as the solid fraction ϕ increases, the flow index n decreases until some critical solid fraction is reached. Above this critical solid fraction a concomitant increase of yield stress τ_0 is evident. We associate this critical solid fraction with the parameter ϕ_* in the *Costa et al.* [2009] model.

[35] Figure 3 shows the variation of η_r values for different kinds of suspensions. The A+B type (spheres plus fibers) and C+D type (SiC plus wollastonite) suspensions show a different behavior of the flow index (n decreases, then increases) with respect to the bimodal spheres blend (A+E type) for which n monotonically decreases. This confirms the first order effect of the particle aspect ratio on the flow properties of a given suspension also for polydisperse mixtures.

[36] Experiments performed on natural basalts with different percentages of crystallized plagioclase by *Ishibashi* [2009] and *Vona et al.* [2011] show a deviation of the flow index n from $n = 1$ at a critical solid fraction around 0.1. This is very similar to the rheological behavior of our suspensions of elongated particles (B type and D type), which show shear thinning behavior for values of $\phi = 0.1$ (for comparison, the average aspect ratio for B-type and D-type particles is 9.5 and 8.5, respectively, whereas the aspect ratio of plagioclase crystals in the experiments of *Vona et al.* [2011] is about 7–8). Moreover, fitting experimental data of natural basalts with equation (4), *Vona et al.* [2011] found the following values for the empirical parameters: $\phi_* = 0.274$, $\xi = 0.0327$, $\gamma = 0.84$ (with $\delta = 13 - \gamma$). These values are very similar to those obtained for the parameterization of the suspension made of monodisperse wollastonite particles (D type in Table 2). This suggests that the analog experiments we performed are able to capture the first order effect of crystals concentration on rheology of magmas.

[37] The critical fraction ϕ_* corresponds to the limit where particle-particle interaction is not negligible anymore and the overall arrangement of the suspended particles reaches a jammed condition. Each

particle has to overcome the resistance of its direct neighbors to move and reorient according to the shear. This causes the onset and increase of the yield stress at increasing solid fraction. Above the critical fraction, only reorientation and reorganization of the particles allows the system to flow. The reorganization of the particles is well illustrated by the texture observed in the epoxy experiment.

[38] Although particle-particle interaction seems to become important above a critical value of ϕ, the similarities between the results obtained for A+B and C+D blends show that the effect of particle surface roughness on the flow properties of the suspensions is negligible (Figures 2 and 3). This suggests that in random packing the maximum spherical orbit of a rotating particle is a pivotal parameter dictating where the threshold of particle-particle interaction is set. On the other hand, the geometry of the suspended particles has a direct influence on the flow index n. It is important to remark that in almost all the suspensions studied, the flow index n above the critical solid fraction inverts its trend and its value increases again toward more Newtonian (n = 1) values.

[39] As a consequence of this nonmonotonic variation of the flow index above the critical fraction, the effective relative viscosity displays a different trend showing a more or less marked inflection, i.e., for a given strain rate, the effective viscosity increases at a slower rate with increasing particle volume above the critical solid fraction. This inflection is more pronounced for high strain rates and for particles with larger aspect ratios such as carbon fibers and wollastonite crystals (types B and D, respectively) and their bimodal blends (A+B and C+D, respectively).

[40] The reorientation of particles in the flow is clearly demonstrated in the epoxy experiment. In particular, the reorganization is effective in creating shear bands and a particle-depleted region proximal to the spindle (Figure 6). This effect is observed both in natural magmas feeding dykes or sills [*Gibb*, 1968; *Nkono et al.*, 2006] and in suspension rheology experiments [*Bramhall and Hutton*, 1960; *Bhattacharji and Smith*, 1964], and consists of a reduction in concentration of the suspended particles adjacent to the solid wall due to the migration of particles from regions of higher shear rate to regions of lower shear rate. In our epoxy experiment, as the suspension is close to the maximum random packing, the depletion of solid particles in high-shear regions is caused by a redistribution of the coarser particles, i.e., their migration toward lower-shear regions. This leads to the formation of a layer with an almost monodisperse distribution of fine particles. As a consequence, a less viscous layer is formed near the wall. This rearrangement of the solid phase can be explained in the light of forces acting on the single particles at the wall margin [*Maude and Withmore*, 1956] and/or as due to the grain dispersive pressure [*Bagnold*, 1954].

[41] The formation of sphere-depleted shear bands, especially near the wall (Figure 6e), produces preferential pathways for the liquid phase to flow. This effect would explain the increase of the effective flow index with increasing solid fraction, i.e., the nonmonotonic trend characterizing the flow index of the nonisometric particle suspensions. This effect is more evident for particles with high aspect ratio that are able to reorient themselves along shear planes and create space sufficient to be occupied by the larger spheres which can rearrange themselves in lower energy configurations. This interpretation is further supported by the observation that the more elongated the particles, the lower the solid fraction at which the flow index n starts to increase and the yield stress to increase notably. This behavior is much less pronounced for monodisperse and bimodal suspensions made from spheres only. An explanation for this is to be found in the packing properties of particles with different symmetry. In fact suspensions of spheres allow higher maximum random packing than anisometric particles do. In contrast to spherical particles, prolate and oblate particles can make available some free volume by reorientating themselves under a given shear.

[42] The considerations made so far have involved solid suspensions that are a simplification of natural magmas. The main simplifications are the absence of a gas phase and the strictly Newtonian rheology of the liquid phase. Nonetheless, many features observed in the concentric cylinder experiment reveal common characteristics with natural volcanic and subvolcanic textures and, to some extent, they share also common aspects with textures of some high-grade metamorphic rocks. For example, the perturbation of foliation planes of smaller crystals in the vicinity of phenocrysts [*Manga*, 1998] or inclusions (or rigid porphyroclasts in the case of metamorphic rocks [*Passchier and Trouw*, 2005]), and the alignment of phenocrysts along shear planes, observed in dykes and lavas [*Smith*, 2002] is well reproduced in the texture of our epoxy analog (Figure 7).

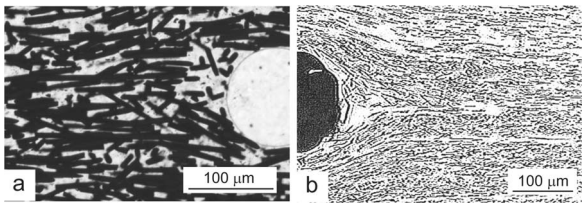

Figure 7. Comparison between (a) the texture obtained in the epoxy experiments and (b) the texture of a natural obsidian flow (modified after *Manga* [1998]). The flow pattern described by elongated microlites around a rounded-shaped phenocryst in the obsidian flow is well reproduced by the carbon fibers around the glass spheres in the experiment.

[43] In a magma undergoing simple shear, sets of crystals with different aspect ratio develop different subfabrics (crystal preferred orientations) according to the rates of rotation around their pivotal axis [*Fernandez et al.*, 1983]. In fact, given a certain amount of strain, crystals with lower aspect ratios will rotate more rapidly toward the shear plane so that the angle defined between the shear direction and the average axis of the fabric would be smaller than that of crystals with higher aspect ratios. Although in concentrated suspensions particle-particle interaction is expected, given a high total strain imparted to the suspension, imbrication of particles is not frequently observed so that foliation direction is commonly parallel to the shear direction (Figure 6). This may not be the case in systems were randomly oriented particles are subject to a quasi-instantaneous deformation. For example, in magmatic systems undergoing rapid application of pressure and shear stress perturbations, the magmatic suspension may not have sufficient time to reorganize and relax under the new flow conditions. Consequently its relaxation threshold can be overcome [*Dingwell*, 1996], with direct implications for the flow and the fragmentation of the magma.

[44] Our experiments also show that for very concentrated bimodal suspensions grain dispersive pressure is effective in establishing both concentration and grain size distribution profiles of crystals. The distribution profile is such that the magmatic flow is depleted in crystals at the edges and enriched in the middle. This causes changes in the rheological profile perpendicularly to the shear flow, with smaller viscosity near the wall where the crystal concentration is lower. Such changes have been proven to affect the velocity profile of flowing magma favoring a plug flow profile instead of a parabolic one both in dykes and lavas [*Komar*, 1972; *Ventura et al.*, 1996]. Effects arising from the temperature gradient within the flow (i.e., viscous heating at the walls and crystal resorption due to the local temperature rise), which are not taken into account in this study, would further complicate the behavior of magmas flowing in conduits and dykes [*Costa et al.*, 2007]. In addition, it is worth mentioning that segregation of crystals entrained in the flow, according to their dimensions and aspect ratio, is also an effective way to promote chemical zonation of the flow, as observed in cooling lava flows and intrusive bodies [*Philpotts et al.*, 1998; *Kuritani et al.*, 2010].

5. Conclusions

[45] Our experiments confirm the pivotal effect of the total solid fraction in affecting the rheology of the investigated suspension and the ability of crystals with higher aspect ratio to anticipate non-Newtonian effects at lower solid fractions compared to more equant ones. In our experiments we have verified that shape variability of natural crystals can be simplified by adopting solid particles with simpler symmetry (spheres, rods) when the aspect ratios of the particles reflects that of the crystals in a magma. Nevertheless, flow curves illustrate that progressive increase of prolate microlites to equant phenocrysts-bearing magma can increase the relative viscosity of up to three orders of magnitude when crystallinity reaches $\phi = 0.4$ or even less. Moreover, our results show that the effect of shape polymodality and size polydistribution of crystals in magmas cannot be resolved by simply modeling the solid phase as a monodisperse population of particles. In particular the difference in aspect ratio between crystals of different size (or different crystal generations), such as phenocrysts and microlites, has to be taken into account as it directly affects the behavior of the suspension under shear. The commonly observed formation of shear bands in magmatic flows is an example of such an effect. Particle depletion and localization of the strain, near the walls, can be responsible for an apparent shear thinning behavior in crystal rich magmas. At the same time this process can have direct consequences on the velocity profile of the flowing magma favoring a plug flow instead of a parabolic one.

Acknowledgments

[46] Financial support to C.C. was provided by the Accademia dei Lincei-Royal Society Fellowship and by Marie Curie

Research Grant "BEACon" 235338. Critical reading of the manuscript by J. Hanson and constructive criticism of two anonymous reviewers improved the final version of the manuscript.

References

Andronico, D., A. Cristaldi, P. Del Carlo, and J. Taddeucci (2009), Shifting styles of basaltic explosive activity during the 2002–03 eruption of Mt. Etna, Italy, *J. Volcanol. Geotherm. Res.*, *180*, 110–122, doi:10.1016/j.jvolgeores.2008.07.026.

Bagnold, R. A. (1954), Experiments on a gravity-free dispersion of large solid spheres in a Newtonian fluid under shear, *Proc. R. Soc. Lond., Ser. A*, *225*, 49–63, doi:10.1098/rspa.1954.0186.

Balmforth, N. J., and R. V. Craster (2001), Geophysical aspects of non-Newtonian fluid mechanics, *Lect. Notes Phys.*, *582*, 34–51.

Bhattacharji, S., and C. H. Smith (1964), Flowage differentiation, *Science*, *145*, 150–153, doi:10.1126/science.145.3628.150.

Bramhall, A. D., and J. F. Hutton (1960), Wall effect in the flow of lubricating greases in plunger viscometers, *Br. J. Appl. Phys.*, *11*, 363–371, doi:10.1088/0508-3443/11/8/312.

Caricchi, L., L. Burlini, P. Ulmer, T. Gerya, M. Vassalli, and P. Papale (2007), Non-Newtonian rheology of crystal-bearing magmas and implications for magma ascent dynamics, *Earth Planet. Sci. Lett.*, *264*, 402–419, doi:10.1016/j.epsl.2007.09.032.

Chong, J., E. Christiansen, and A. Baer (1971), Rheology of concentrated suspension, *J. Appl. Polym. Sci.*, *15*, 2007–2021, doi:10.1002/app.1971.070150818.

Cimarelli, C., F. Di Traglia, and J. Taddeucci (2010), Basaltic scoria textures from a zoned conduit as precursors to violent Strombolian activity, *Geology*, *38*(5), 439–442, doi:10.1130/G30720.1.

Costa, A. (2005), Viscosity of high crystal content melts: Dependence on solid fraction, *Geophys. Res. Lett.*, *32*, L22308, doi:10.1029/2005GL024303.

Costa, A., O. Melnik, and E. Vedeneeva (2007), Thermal effects during magma ascent in conduits, *J. Geophys. Res.*, *112*, B12205, doi:10.1029/2007JB004985.

Costa, A., L. Caricchi, and N. Bagdassarov (2009), A model for the rheology of particle-bearing suspensions and partially molten rocks, *Geochem. Geophys. Geosyst.*, *10*, Q03010, doi:10.1029/2008GC002138.

Dingwell, D. B. (1996), Volcanic dilemma: Flow or blow?, *Science*, *273*, 1054–1055, doi:10.1126/science.273.5278.1054.

Farris, R. J. (1968), Prediction of the viscosity of multimodal suspensions from unimodal viscosity data, *Trans. Soc. Rheol.*, *12*(2), 281–301, doi:10.1122/1.549109.

Fernandez, A., J. L. Feybesse, and J. F. Mezure (1983), Theoretical and experimental study of fabrics developed by different shaped markers in two-dimensional simple shear, *Bull. Soc. Geol. Fr.*, *7*(25), 319–326.

Gibb, F. G. F. (1968), Flow differentiation in the xenolithic ultrabasic dykes of the Cuillins and the Strathaird Peninsula, Isle of Skye, Scotland, *J. Petrol.*, *9*, 411–443.

Giordano, D., J. K. Russel, and D. B. Dingwell (2008), Viscosity of magmatic liquids: A model, *Earth Planet. Sci. Lett.*, *271*, 123–134, doi:10.1016/j.epsl.2008.03.038.

Hammer, J. E., K. V. Cashman, R. P. Hoblitt, and S. Newman (1999), Degassing and microlite crystallization during pre-climactic events of the 1991 eruption of Mt. Pinatubo, Philippines, *Bull. Volcanol.*, *60*, 355–380, doi:10.1007/s004450050238.

Herschel, W. H., and R. Bulkley (1926), Konsistezmessungen von gummi-benzol-loesungen, *Colloid Polym. Sci.*, *39*, 291–300, doi:10.1007/BF01432034.

Houghton, B. F., and H. M. Gonnermann (2008), Basaltic explosive volcanism: Constraints from deposits and models, *Chem. Erde*, *68*(2), 117–140, doi:10.1016/j.chemer.2008.04.002.

Ishibashi, H. (2009), Non-Newtonian behavior of plagioclase-bearing basaltic magma: Subliquidus viscosity measurement of the 1707 basalt of Fuji volcano, Japan, *J. Volcanol. Geotherm. Res.*, *181*, 78–88, doi:10.1016/j.jvolgeores.2009.01.004.

Ishibashi, H., and H. Sato (2007), Viscosity measurements of subliquidus magmas: Alkali olivine basalt from the Higashi-Matsuura district, Southwest Japan, *J. Volcanol. Geotherm. Res.*, *160*, 223–238, doi:10.1016/j.jvolgeores.2006.10.001.

Komar, P. D. (1972), Mechanical interactions of phenocrysts and flow differentiation of igneous dikes and sills, *Geol. Soc. Am. Bull.*, *83*, 973–988.

Krieger, I., and T. Dougherty (1959), A mechanism for non-Newtonian flow in suspension of rigid spheres, *Trans. Soc. Rheol.*, *3*, 137–152, doi:10.1122/1.548848.

Kuritani, T., T. Yoshida, and Y. Nagahashi (2010), Internal differentiation of Kutsugata lava flow from Rishiri Volcano, Japan: Processes and timescales of segregation structures' formation, *J. Volcanol. Geotherm. Res.*, *195*, 57–68, doi:10.1016/j.jvolgeores.2010.06.003.

Lejeune, A., and P. Richet (1995), Rheology of crystal-bearing silicate melts: An experimental study at high viscosity, *J. Geophys. Res.*, *100*, 4215–4229, doi:10.1029/94JB02985.

Manga, M. (1998), Orientation distribution of microlites in obsidian, *J. Volcanol. Geotherm. Res.*, *86*, 107–115, doi:10.1016/S0377-0273(98)00084-5.

Marti, I., O. Höfler, P. Fischer, and E. J. Windhab (2005), Rheology of concentrated suspensions containing mixtures of spheres and fibres, *Rheol. Acta*, *44*, 502–512, doi:10.1007/s00397-005-0432-9.

Maude, A. D., and R. L. Withmore (1956), The wall effect and the viscometry of suspensions, *Br. J. Appl. Phys.*, *7*, 98–102, doi:10.1088/0508-3443/7/3/305.

McBirney, A. R., and T. Murase (1984), Rheological properties of magma, *Annu. Rev. Earth Planet. Sci.*, *12*, 337–357, doi:10.1146/annurev.ea.12.050184.002005.

Mueller, S., E. Llewellin, and H. M. Mader (2010), The rheology of suspensions of solid particles, *Proc. R. Soc. A*, *466*, 1201–1228, doi:10.1098/rspa.2009.0445.

Nkono, C., O. Féménias, D. Hervé, T. Berza, and D. Demaiffe (2006), Flowage differentiation in an andesitic dyke of the Motru Dyke Swarm (Southern Carpathians, Romania) inferred from AMS, CSD and geoghemistry, *J. Volcanol. Geotherm. Res.*, *154*, 201–221, doi:10.1016/j.jvolgeores.2006.02.011.

Noguchi, S., A. Toramaru, and T. Stimano (2006), Crystallization of microlites and degassing during magma ascent: Constraints on the fluid mechanical behaviour of magma during the Tenjo Eruption on Kozu Island, Japan, *Bull. Volcanol.*, *68*, 432–449.

Passchier, C. W., and R. A. J. Trouw (2005), *Microtectonics*, 366 pp., Springer, Berlin.

Petford, N. (2003), Rheology of granitic magmas during ascent and emplacement, *Annu. Rev. Earth Planet. Sci.*, *31*, 399–427, doi:10.1146/annurev.earth.31.100901.141352.

Petford, N. (2009), Which effective viscosity?, *Mineral. Mag.*, *73*, 167–191, doi:10.1180/minmag.2009.073.2.167.

Philpotts, A. R., J. Shi, and C. Brustman (1998), Role of plagioclase crystal chains in the differentiation of parlty crystallized basaltic magma, *Nature*, *395*, 343–346, doi:10.1038/26404.

Pinkerton, H., and R. Stevenson (1992), Methods of determining the rheological properties of magmas at sub-solidus temperatures, *J. Volcanol. Geotherm. Res.*, *53*, 47–66, doi:10.1016/0377-0273(92)90073-M.

Sable, J. E., B. F. Houghton, P. Del Carlo, and M. Coltelli (2006), Changing conditions of magma ascent and fragmentation during the Etna 122 BC basaltic Plinian eruption: Evidence from clast microtextures, *J. Volcanol. Geotherm. Res.*, *158*, 333–354, doi:10.1016/j.jvolgeores.2006.07.006.

Smith, J. V. (2002), Structural analysis of flow-related textures in lavas, *Earth Sci. Rev.*, *57*, 279–297, doi:10.1016/S0012-8252(01)00081-2.

Sparks, R. S. J. (1997), Causes and consequences of pressurisation in lava dome eruptions, *Earth Planet. Sci. Lett.*, *150*(3–4), 177–189, doi:10.1016/S0012-821X(97)00109-X.

Spera, F. J. (2000), Physical properties of magma, in *Encyclopedia of Volcanoes*, edited by H. Sigurdsson, pp. 171–190, Academic, San Diego, Calif.

Stickel, J. J., and R. L. Powell (2005), Fluid mechanics and rheology of dense suspensions, *Annu. Rev. Fluid Mech.*, *37*, 129–149, doi:10.1146/annurev.fluid.36.050802.122132.

Suzuki, Y., and T. Fujii (2010), Effect of syneruptive decompression path on shifting intensity in basaltic sub-Plinian eruption: Implication of microlites in Yufune-2 scoria from Fuji volcano, Japan, *J. Volcanol. Geotherm. Res.*, *198*, 158–176, doi:10.1016/j.jvolgeores.2010.08.020.

Szramek, L., J. E. Gardner, and J. Larsen (2006), Degassing and microlite crystallization of basaltic andesite magma erupting at Arenal Volcano, Costa Rica, *J. Volcanol. Geotherm. Res.*, *157*, 182–201, doi:10.1016/j.jvolgeores.2006.03.039.

Toramaru, S., S. Noguchi, A. Oyoshihara, and A. Tsune (2008), MND (microlite number density) water exsolution rate meter, *J. Volcanol. Geotherm. Res.*, *175*, 156–167, doi:10.1016/j.jvolgeores.2008.03.035.

Ventura, G., R. De Rosa, R. Mazzuoli, and E. Colletta (1996), Deformation patterns in high-viscous lava flows inferred from the preferred orientation and tiling of crystals. An example from Salina (Aeolian Islands, Southern Tyrrhenian Sea, Italy), *Bull. Volcanol.*, *57*, 555–562.

Vona, A., C. Romano, D. B. Dingwell, and D. Giordano (2011), The rheology of crystal-bearing basaltic magmas from Stromboli and Etna, *Geochim. Cosmochim. Acta*, *75*, 3214–3236, doi:10.1016/j.gca.2011.03.031.